ELSEVIER

Earth and Planetary Science Letters 192 (2001) 347–361

EPSL

www.elsevier.com/locate/epsl

Anisotropy of oxygen diffusion in diopside

Jannick Ingrin *, Laure Pacaud, Olivier Jaoul

Minéralogie, Laboratoire Mécanismes de Transfert en Géologie, CNRS UMR-5563, Université Paul Sabatier, 39 Allées Jules Guesde, F-31000 Toulouse, France

Received 25 April 2001; received in revised form 20 June 2001; accepted 26 July 2001

Abstract

^{18}O diffusion coefficients have been measured by nuclear reaction analysis (NRA) in Fe-free synthetic diopside single crystals along the three crystallographic directions and in Fe-bearing natural diopside single crystals along the *c* direction at room pressure in the range 1050–1370°C and under controlled oxygen partial pressure (10^{-3}–10^{-12} atm). Diffusion along *a* and *c* crystallographic directions is one order of magnitude faster than along *b* direction. Diffusion along *c* in natural diopside is about two times faster than in the synthetic sample. The activation energy along *b* is 323 ± 27 kJ mol^{-1} and diffusion is insensitive to oxygen fugacity. For *a* and *c* directions activation energies are around 250 kJ mol^{-1} and the diffusion coefficients are slightly dependent on fO_2 ($\approx fO_2^{0.04}$). We suggest that the observed diffusion anisotropy is related to the oxygen diffusion paths within the crystallographic structure that prefer the under-bonded O2 oxygen sites. We propose a single law to describe diffusion along the two fast crystallographic directions *a* and *c* in diopside for natural conditions close to the QFM buffer:

$$\log D_{a,c}\ (\mathrm{m^2\ s^{-1}}) = -10.0 \pm 0.6 - (259 \pm 15\ \mathrm{kJ\ mol^{-1}})/2.303\ RT,\ \textit{and}\ D_b \ll D_{a,c}$$

Keywords: oxygen; diffusion; diopside; O-18/O-16; cooling

1. Introduction

Oxygen isotopes are frequently used to determine the peak temperature of a metamorphic event, providing that no isotopic resetting happens during the retrograde metamorphic path of the rock. When partial re-equilibration of oxygen isotopes occurs during cooling of a metamorphic terrain, it is theoretically possible to deduce the rate of cooling from the oxygen isotope disequilibrium measured within one or several mineral phases [1–3]. The approach has been applied with success to compute the cooling rate of slowly cooled metamorphic rocks from the Adirondack [4,5]. However, despite a recent improvement of the technique based on the use of the compensation rule [6], such analyses, trying to extract cooling rates from the measurements of closure temperatures in grains of various sizes, are still very dependent on the extrapolations at low temperature of diffusion coefficients measured in laboratory. For these reasons, we need to have a good understanding of the microscopic mechanisms in-

* Corresponding author. Tel.: +33-561558015; Fax: +33-561558023.
E-mail address: ingrin@cict.fr (J. Ingrin).

0012-821X/01/$ – see front matter
PII: S0012-821X(01)00460-5

Table 1
Diffusion data of synthetic iron-free diopside

Run (no.)	T (°C)	Duration (h)	fO_2 (atm)	$2\sqrt{Dt}$ (nm)	D (m^2/s)	C_0
Diffusion along the *b* direction						
i5	1250	110	1.6×10^{-12}	110	7.6×10^{-21}	0.15
f5	1250	144	6.7×10^{-11}	160	1.2×10^{-20}	0.015
e4	1300	138	1×10^{-10}	270	3.7×10^{-20}	0.05
c2[a]	1350	96	9.4×10^{-10}	380	1×10^{-19}	0.01
Diffusion along the *c* direction						
r7	1050	222	6.8×10^{-2}	160	8×10^{-21}	0.05
l2	1140	192	6.8×10^{-2}	305	3.4×10^{-20}	0.06
o1	1140	360	6.3×10^{-2}	400	3.1×10^{-20}	0.07
m4	1170	47.5	3×10^{-2}	150	3.3×10^{-20}	0.06
s4	1170	71.5	3×10^{-2}	250	6.1×10^{-20}	0.05
r4	1200	48	3×10^{-2}	250	9×10^{-20}	0.12
r5	1200	56	8.2×10^{-2}	300	1.1×10^{-19}	0.08
o6	1200	64	2.2×10^{-2}	370	1.5×10^{-19}	0.045
q1	1200	144	7.4×10^{-2}	500	1.2×10^{-19}	0.05
m2	1200	456	7.7×10^{-2}	900	1.2×10^{-19}	0.05
l5	1200	23	2×10^{-11}	130	5.1×10^{-20}	0.05
l7	1250	48	5.8×10^{-2}	380	2.1×10^{-19}	0.07
o7	1250	55.5	5.8×10^{-2}	480	2.9×10^{-19}	0.03
r1	1250	168	7.2×10^{-2}	640	1.7×10^{-19}	0.1
k1	1250	360	1×10^{-2}	750	1.1×10^{-19}	0.04
m3	1250	72	6.7×10^{-11}	300	8.7×10^{-20}	0.02
n1	1250	175	1.5×10^{-10}	400	6.3×10^{-20}	0.05
m7	1300	45	3.5×10^{-2}	560	4.8×10^{-19}	0.05
m6[a]	1300	52	9.5×10^{-2}	580	4.5×10^{-19}	0.07
o4	1300	52	9.5×10^{-2}	590	4.6×10^{-19}	0.05
p1[a]	1300	72	4.5×10^{-2}	360	1.2×10^{-19}	0.07
r2[a]	1300	144	4.5×10^{-2}	610	1.8×10^{-19}	0.06
l3	1300	72.5	6×10^{-12}	240	5.5×10^{-20}	0.06
o2	1300	96	1.2×10^{-10}	410	1.2×10^{-19}	0.04
l8[a]	1330	19	1.1×10^{-2}	420	6.4×10^{-19}	0.05
p2[a]	1330	48	5.3×10^{-9}	450	2.9×10^{-19}	0.013
m1	1350	24	2.4×10^{-2}	320	3×10^{-19}	0.03
s5[a]	1350	27.3	4.3×10^{-2}	450	5.1×10^{-19}	0.1
l1	1350	48	5×10^{-2}	480	3.3×10^{-19}	0.015
s1	1350	96	7.5×10^{-2}	630	2.9×10^{-19}	0.1
s2[a]	1350	24	1.3×10^{-9}	320	3×10^{-19}	0.02
l6	1350	24.3	1.2×10^{-9}	230	1.5×10^{-19}	0.15
l9	1350	56	1.7×10^{-9}	780	7.5×10^{-19}	0.04
m5[a]	1370	24	5.1×10^{-2}	450	5.9×10^{-19}	0.15
Diffusion along the *a* direction						
v4	1050	176	6.8×10^{-2}	100	3.9×10^{-21}	0.03
t2	1200	64	2.2×10^{-2}	220	5.2×10^{-20}	0.05
v3	1250	48.5	5.8×10^{-2}	250	8.9×10^{-20}	0.03
t3	1250	55.5	5.8×10^{-2}	350	1.5×10^{-19}	0.04
u1	1250	110	1.6×10^{-12}	150	1.4×10^{-20}	0.15
v1	1250	136	1.6×10^{-12}	130	8.6×10^{-21}	0.15
w1	1300	45	3.5×10^{-2}	430	2.8×10^{-19}	0.055
v2	1300	45	2.6×10^{-2}	300	1.4×10^{-19}	0.06
t1	1300	97	3.5×10^{-2}	620	2.7×10^{-19}	0.04
w2	1350	30	2×10^{-2}	450	4.7×10^{-19}	0.05
t4	1350	56	1.7×10^{-9}	420	2.2×10^{-19}	0.12

volved in oxygen diffusion in minerals, as in the present case, for diopside.

Oxygen diffusion in single crystal diopsides has been the subject of several experimental works [3,7–9]. Important discrepancies exist between the reported data. Their extrapolations down to 700°C span nearly seven orders of magnitude (Fig. 1). Several questions regarding the diffusion of oxygen in diopside still remain unsolved. For instance, an anisotropy has been observed between the *c* crystallographic direction and an unknown direction perpendicular to *c* [3]. One of the aims of this paper is to check and quantify the effect of anisotropy and try to understand the crystallographic origin of this anisotropy.

The effect of water on diffusion is also subject to debate: some evidence of water enhancement has been proposed from field observations [4,10], but experimental data are scattered (compare data resulting from dry condition and hydrothermal experiments; Fig. 1). An other purpose of the paper is to implement the existing data collected from dry conditions experiments in order to consolidate comparison with hydrothermal data.

In this paper, we present new data on oxygen diffusion obtained from experiments performed at atmospheric pressure in iron-free single synthetic diopside oriented along *b*, *c* and *a* crystallographic directions and along *c* in a natural crystal. Simple crystallographic considerations will be used to explain the observed anisotropy of diffusion in terms of diffusion paths. Finally, we propose a common average law for the diffusion of oxygen in diopsides, along the two rapid directions *a* and *c*.

2. Experimental and analytical procedures

The description below is restricted to information critical for understanding the present results and their discussion. Details of the experimental and analytical procedures are reported in [9,11].

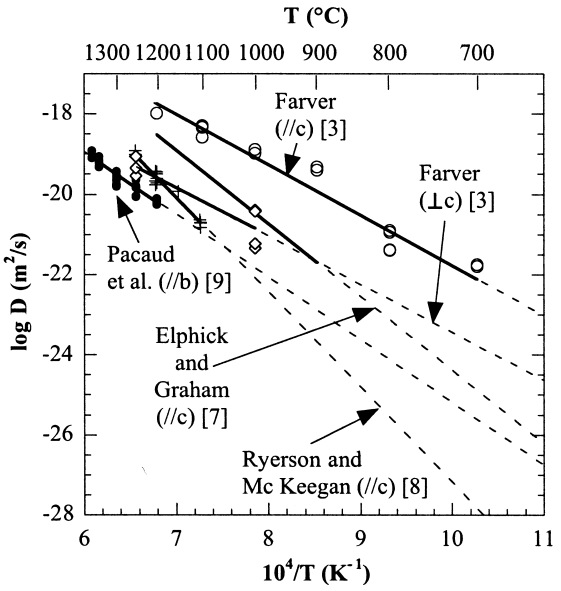

Fig. 1. Arrhenius plot log D (m^2 s^{-1}) versus $10^4/T$ (K^{-1}) of previous oxygen diffusion data collected from single crystal diopsides. Experimental data (symbols); linear fit (full lines) and their extrapolations toward lower temperature (dashed lines) are reported. No data points were reported in [7]. Data [3,7] are from hydrothermal runs and data [8,9] are 1 atm 'dry' experiments.

2.1. Synthetic diopside

The synthetic samples used are identical to those studied in [9,12]. The chemical composition determined by electron microprobe gives $Ca_{0.950\pm0.007}Mg_{1.050\pm0.007}Si_{1.996\pm0.005}O_6$ (with Fe-content below the detection limit, <0.003). Specimens were oriented using the X-ray Laüe technique within a precision of 5°, with their larger faces perpendicular to [010], [001] and to an axis at 13° from the [100] direction toward the [00-1] direction (respectively labelled *b*, *c* and *a*; Table 1). The thin slices, around 6 mm^2 area, 1 mm thick, were polished with alumina powder down to 0.3 μm. After polishing, the slices were etched in hydrofluoric acid, diluted to 50%, in order to

←

Samples are labelled by letters a, b, ..., the number which follows corresponds to the succession of annealing runs of the same specimen [9].

[a]Thermal etch pits observed at the surface of the sample.

remove the cold-worked zone produced at the surface by mechanical polishing.

For nuclear reaction analysis (NRA) and Rutherford backscattering spectrometry analysis (RBS), the annealed samples were glued on copper supports and a thin film of amorphous carbon was evaporated on the surface to avoid charging during ion beam irradiation in the accelerator.

2.2. Natural diopside

The thin slices of Russian diopside used for the study were cut in a diopside single crystal from the same origin as the one used in [13]. The average composition is $Ca_{0.969}Na_{0.025}Mg_{0.970}Fe_{0.036}Cr_{0.013}Al_{0.007}Si_{1.987}O_6$. The size of the thin slices and the procedure followed for the sample preparation was identical as for the synthetic samples.

2.3. Samples annealing

The experimental conditions for oxygen diffusion experiments were identical as in [9]. Runs were performed in a horizontal alumina tubing externally heated by a lanthanum chromite resistor (Pyrox, VG 30 furnace). The temperature range of experiments was 1050–1370°C. Synthetic samples were placed in a platinum crucible on an alumina plate in the center part of the furnace. Natural samples were placed in a polycrystalline diopside crucible, the whole being put on a MgO plate that was in turn placed on an alumina plate. Temperature was controlled within less than ± 5°C. Heating and cooling durations (about 1 h in total) were short compared to annealing durations so that the diffusion profiles were not significantly affected.

Diffusion of ^{18}O tracer was performed by a direct gas–solid exchange between an ^{18}O-enriched atmosphere and the polished samples surface. The isotopic source for tracer diffusion is a controlled mixture of argon and H_2 flowing through ^{18}O-enriched water. The ^{18}O-enriched water contained in the gas after its travel through the furnace was freeze-dried at −10°C for reuse after experiment. Thus, the amount of enrichment is not identical for each experiment, producing an isotopic covering rate of the diopside surface (C_0) ranging between 15% and 1% (Tables 1 and 2). The resulting H_2O vapor pressure ($pH_2O = 0.026$

Table 2
Diffusion data of natural Fe-bearing diopside

Run	T (°C)	Duration (h)	fO_2 (atm)	$2\sqrt{Dt}$ (nm)	D (m^2/s)	C_0
Natural diopside, diffusion along the c direction						
Nc6	1100	78.5	4.1×10^{-2}	250	5.5×10^{-20}	0.07
Nd3	1100	78.5	4.1×10^{-2}	255	5.7×10^{-20}	0.08
Nb2	1150	97.5	4×10^{-2}	310	6.8×10^{-20}	0.1
Nb3	1150	121	2.5×10^{-2}	290	4.8×10^{-20}	0.13
Nb4	1150	76	2.9×10^{-10}	200	3.6×10^{-20}	0.03
Nd2	1200	24	5.2×10^{-2}	220	1.4×10^{-19}	0.12
Nc2	1200	29	5.2×10^{-2}	260	2.8×10^{-19}	0.06
Na3	1200	60.5	7.6×10^{-2}	380	1.7×10^{-19}	0.04
Na1	1240	71	4.5×10^{-2}	460	2×10^{-19}	0.1
Nb1	1240	71	4.9×10^{-2}	490	2.3×10^{-19}	0.07
Nc1	1240	96	4.9×10^{-2}	700	2.4×10^{-19}	0.08
Nd1	1240	143	4.5×10^{-2}	690	2.3×10^{-19}	0.08
Na4	1240	24	1.2×10^{-11}	280	2.3×10^{-19}	0.01
Nc5	1240	49	7.4×10^{-9}	320	1.4×10^{-19}	0.03
Na2	1260	15.5	9.3×10^{-2}	325	4.7×10^{-19}	0.06
Nc3	1260	21	9×10^{-2}	420	5.9×10^{-19}	0.02
Na5	1280	13.5	9.4×10^{-2}	450	1.0×10^{-18}	0.02

Samples are labelled by letters Na, Nb, ..., the number which follows corresponds to the succession of annealing runs of the same specimen [9].

atm at 22°C) mixed with Ar and H_2 imposes fO_2 in the furnace and is monitored by a zirconia probe ($SIRO_2$ sensor). The most oxidizing regime was performed with pure Ar flowing through water, leading to $fO_2 \approx 9.10^{-2}$–1.5×10^{-3} atm, depending on temperature. The most reducing experiments (fO_2 between 10^{-9} and 10^{-12} atm) were obtained with Ar/10%H_2 flowing through water.

After each run, the sample surface was carefully observed with an optical microscope. Except for small thermal etch pits in a few experiments with $T = 1300$°C (Table 1), the surface of the samples remained almost physically unaltered. Each sample was used several times and repolished between each run (Tables 1 and 2; [9]).

2.4. Measurements of oxygen profiles

Systematic RBS analyses, with a beam of 2 MeV α-particles, were performed on samples prior to NRA in order to check the surface chemical composition and isotopic enrichment and, if necessary, slightly change the orientation of the target under the beam to avoid channelling of incident particles along preferential crystallographic orientations.

The concentration profiles of ^{18}O were obtained by the specific ^{18}O nuclear reaction $^{18}O + p \rightarrow \alpha + {}^{15}N$ that is specific to ^{18}O, with a 740 keV incident proton beam, 1–2 mm in diameter (see details on the technique in [9,14]). The energy of the produced α-particles was measured with a germanium detector at an angle of $\theta = -30°$ relative to the incident proton beam. For depths x smaller than 1000 nm, the energy loss ΔE_α of the detected α-particles can be expressed by the linear relation [9]:

$$\frac{\Delta E_\alpha}{\Delta x} = S$$

with the stopping power $S = 0.37$ keV nm^{-1}, with x the depth of the nuclear reaction beneath the surface, and $x = 0$ at the surface.

The NRA spectrum (number of α counts versus their energy or depth of ^{18}O beneath surface, Fig. 2) represents a picture of the ^{18}O concentration as a function of depth.

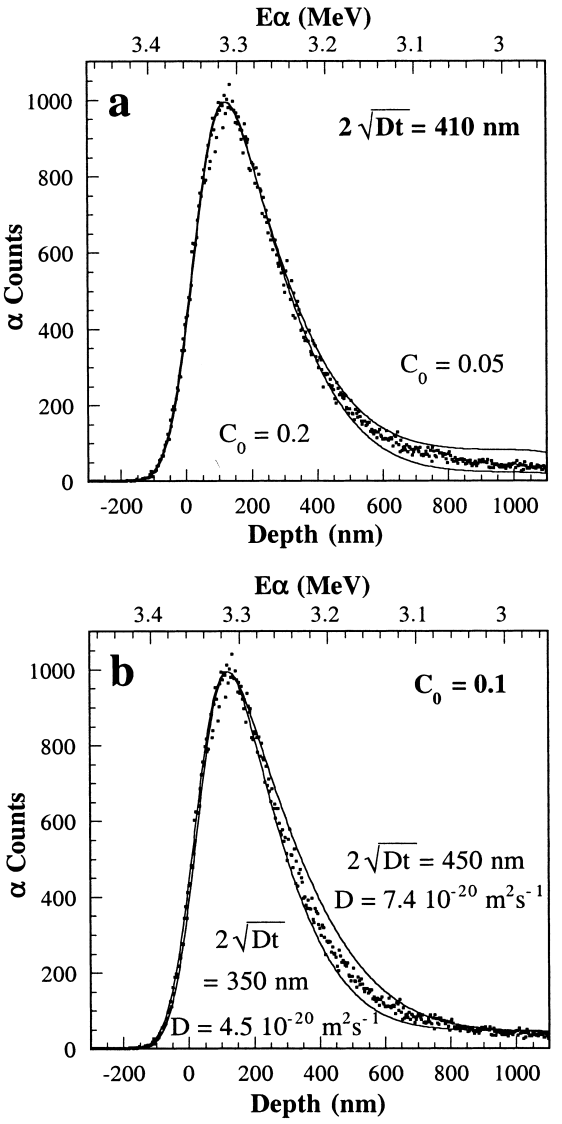

Fig. 2. Experimental NRA profiles and the fitting process for sample f2 annealed for 189 h at 1350°C [9]. (a) Shows the effect of varying C_0 at constant $2\sqrt{Dt}$, and (b) varying $2\sqrt{Dt}$ at constant C_0. One imposes the maximum of the curve to fit the maximum of the α counts.

2.5. Calculation of diffusion coefficients

To extract diffusion coefficients from the oxygen profiles, we performed numerical simulations by convoluting the solution of the diffusion law for a semi-infinite slab Eq. 1 with the instrumental function Eq. 2:

$$C(x,t) = C_\infty + (C_0 - C_\infty)\mathrm{erfc}\left(\frac{x}{2\sqrt{Dt}}\right) \quad (1)$$

where t is the annealing duration, C_∞ is the natural isotopic abundance ($C_\infty = 0.2\%$), C_0 is the isotopic surface concentration fixed by the gas mixture, and erfc is the complementary error function. D is the diffusion coefficient and $2\sqrt{Dt}$ is the diffusion characteristic length which can amount to several hundreds of nanometer. The mathematical solution $C(x)$ obtained after the annealing duration t is in reality convolved with an instrumental Gaussian function linked to the NRA method:

$$G(x) = \frac{1}{\sqrt{2\pi}\sigma}\exp\left(-\frac{x^2}{2\sigma^2}\right) \quad (2)$$

in which σ (nm) = 1/S Σ(keV), where Σ is related to the detector resolution R and the straggling effect T (i.e. energy dispersion):

$$\sigma(x) = \sqrt{(R^2 + xT^2)}$$

In the present study, $R = 23$ keV: it represents the resolution in energy of the detector and corresponds to a resolution in depth of 60 nm. We used the straggling value $T = 0.19$ keV nm$^{-0.5}$ [9,12]. Data were fitted by the function $C(x)$ convoluted with $G(x)$ and by allowing adjustment of the two parameters C_0 and $2\sqrt{Dt}$ (Fig. 2). C_0 has different values in each of our experiments because the enrichment in $H_2^{18}O$ was different, due to the recycling process mentioned earlier.

The oxygen profile of one sample (n1; Table 1) was also measured by secondary ion mass spectrometry (SIMS; analysis performed by F. Azough, R. Freer and J. Craven with the Edinburgh's Cameca IMS-4f ion probe, [11]). The similarity of the results obtained by the two methods, with diffusion characteristic length of 410 nm and 400 nm for the SIMS and the NRA techniques respectively (Table 1) confirms the validity of both techniques to measure such oxygen profiles [15].

2.6. Uncertainties

It is a very delicate discussion that must be rendered as clear as possible if one likes to compare data issued from different laboratories and techniques. There are three different types of uncertainties in diffusion data collection:

1. Each individual annealing run gives rise to a fit of the diffusion profile within the crystal. This 'analytical uncertainty' is generally negligible compared to other sources of errors. For our experiments this uncertainty is of the order of 0.05 log unit for each individual measurement [9].
2. The 'individual experimental uncertainty' is higher than the 'analytical uncertainty' and much more difficult to estimate. It depends on the reproducibility of experimental conditions, the reproducibility of the sample preparation (repolishing after each experiment, carbon coating, ...) and the variability of the samples itself. This uncertainty can be theoret-

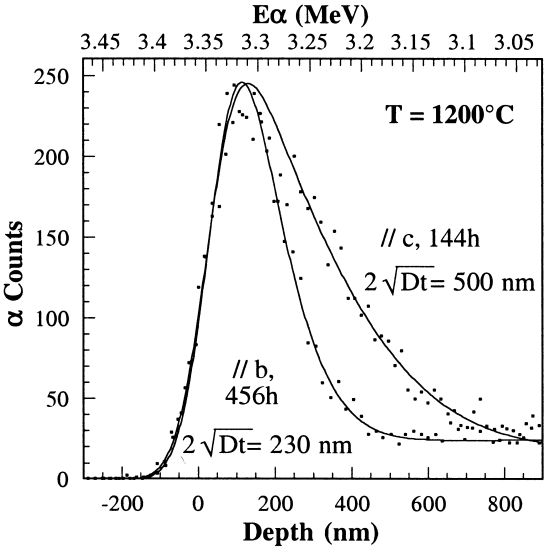

Fig. 3. Experimental NRA profiles and their fit for two samples annealed at $T = 1200$°C. The sample f3 (annealing duration 456 h; [9]) is oriented along b; the sample q1 (annealing duration 144h; Table 1) is oriented along c. The diffusion coefficients deduced from these fits are 8×10^{-21} m^2 s^{-1} and 1.2×10^{-19} m^2 s^{-1} respectively. In both cases $fO_2 \approx 7$–8×10^{-2} atm.

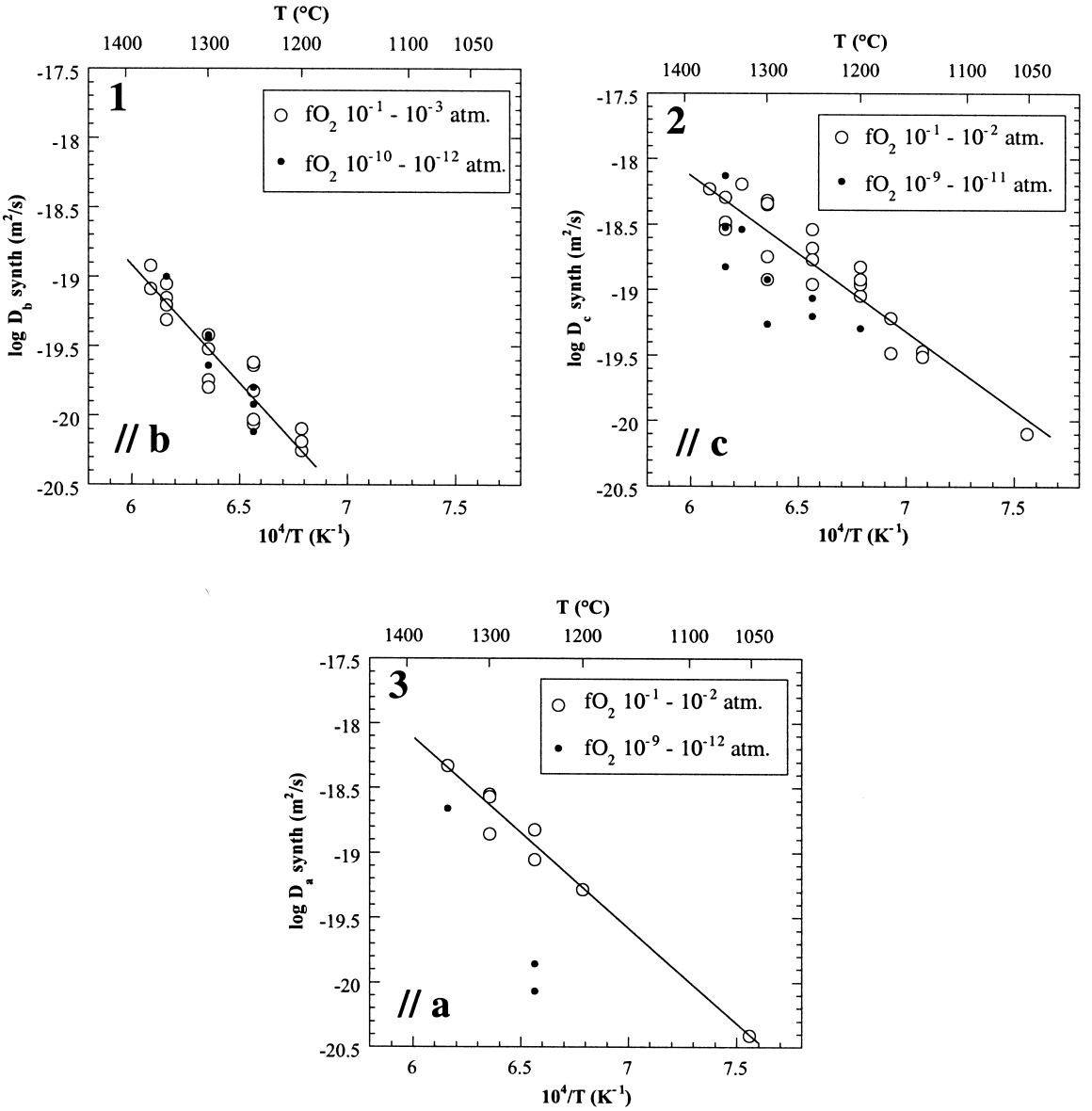

Fig. 4. Arrhenius plot for synthetic samples. Data along *b* (4.1) are from [9] and this study, with linear fit corresponding to Eq. 3. Linear fits for *c* (4.2) and *a* (4.3) directions are only for oxidizing conditions (empty circles), and correspond to Eqs. 4 and 5, respectively. Notice slower diffusion along *b*, by a factor 10, compared to *a* and *c*.

ically estimated from successive runs done at a same temperature. However, a correct measurement of such uncertainty would necessitate an analysis from a statistical representative population of runs performed in the same conditions (at least 30 individual runs). Such procedure is highly time consuming and is rarely followed. In our study the maximum of runs done at same temperature and same fO_2 is 5 and the maximum error observed is generally below ± 0.25 log unit with one single exception (± 0.35 log unit; see figure 5 in [9] and Tables 1 and 2). The long experience of diffusion data acquisition of our laboratory allows us to en-

sure that the 'individual experimental uncertainty' of these techniques is always smaller than ±0.5 log unit. Thus we generally take this value as the uncertainty limit of our individual diffusion data. This error corresponds to a very high level of confidence, of the order of three standard deviations.

3. The uncertainty on the activation energy and on the pre-exponential factor D_0 is the uncertainty on the linear regression used to fit the Arrhenius law. This 'regression uncertainty' is a function of the 'individual experimental uncertainty' but also of the number of data points considered and of the window dimension in $1/T$. The higher the number of experimental data and the larger the temperature range of experiments, the better is the 'regression uncertainty'. In the diffusion laws presented in this report, the uncertainties on the activation energies range from 33 to 15 kJ mol^{-1} for respectively 14 and 51 data sets and temperature ranges of 180°C and 320°C.

3. Results

Temperature, annealing duration, fO_2, $2\sqrt{Dt}$, D the deduced diffusion coefficient and C_0 the isotopic surface concentration of each run are reported in Tables 1 and 2.

3.1. Data

The anisotropy of oxygen diffusion in diopside is clearly demonstrated by comparing diffusion profiles of two samples annealed at 1200°C, one oriented along b and the other along c (Fig. 3). The diffusion characteristic length along c is more than twice that of the other sample despite a much shorter annealing duration. Fig. 4 gives Arrhenius plots obtained for synthetic samples along the three directions. Oxygen diffusion coefficients along c and a have similar values while diffusion along b is more than one order of magnitude slower in this range of temperature.

Experiments on four synthetic samples oriented along b direction have been performed in reducing conditions (samples i5, f5, e4 and c2) (Table 1). Added to data reported in [9] for high and low fO_2 these results definitively confirm the independence of oxygen diffusion with fO_2 along b (Fig. 4.1). The whole set of data yields:

$$\log D_b \text{ synth } (m^2\ s^{-1}) =$$

$$-8.8 \pm 0.9 - (323 \pm 27 \text{ kJ mol}^{-1})/2.303\ RT \quad (3)$$

The fit was performed assuming an individual experimental uncertainty of ±0.5 log unit of D and ±5°C on T [9,16]. Linear regression errors correspond to one standard deviation.

Data for c and a directions of synthetic diopside annealed in oxidizing conditions are similar within the uncertainties (Fig. 4.2, 4.3). We find:

$$\log D_c \text{ synth } (m^2\ s^{-1}) =$$

$$-11 \pm 0.7 - (228 \pm 20 \text{ kJ mol}^{-1})/2.303\ RT \quad (4)$$

$$\log D_a \text{ synth } (m^2\ s^{-1}) =$$

$$-9.3 \pm 0.8 - (281 \pm 21 \text{ kJ mol}^{-1})/2.303\ RT \quad (5)$$

Diffusion coefficients of natural diopside along c are slightly greater than for the synthetic Fe-free

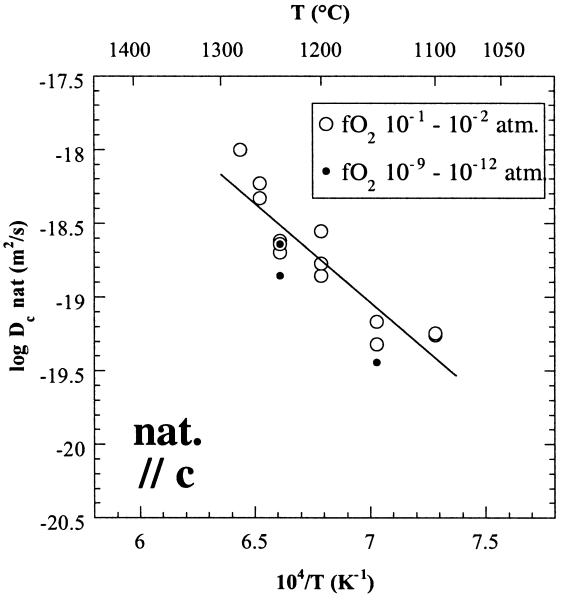

Fig. 5. Arrhenius plot for natural Fe-bearing samples. The fit corresponds to oxidizing conditions, Eq. 6.

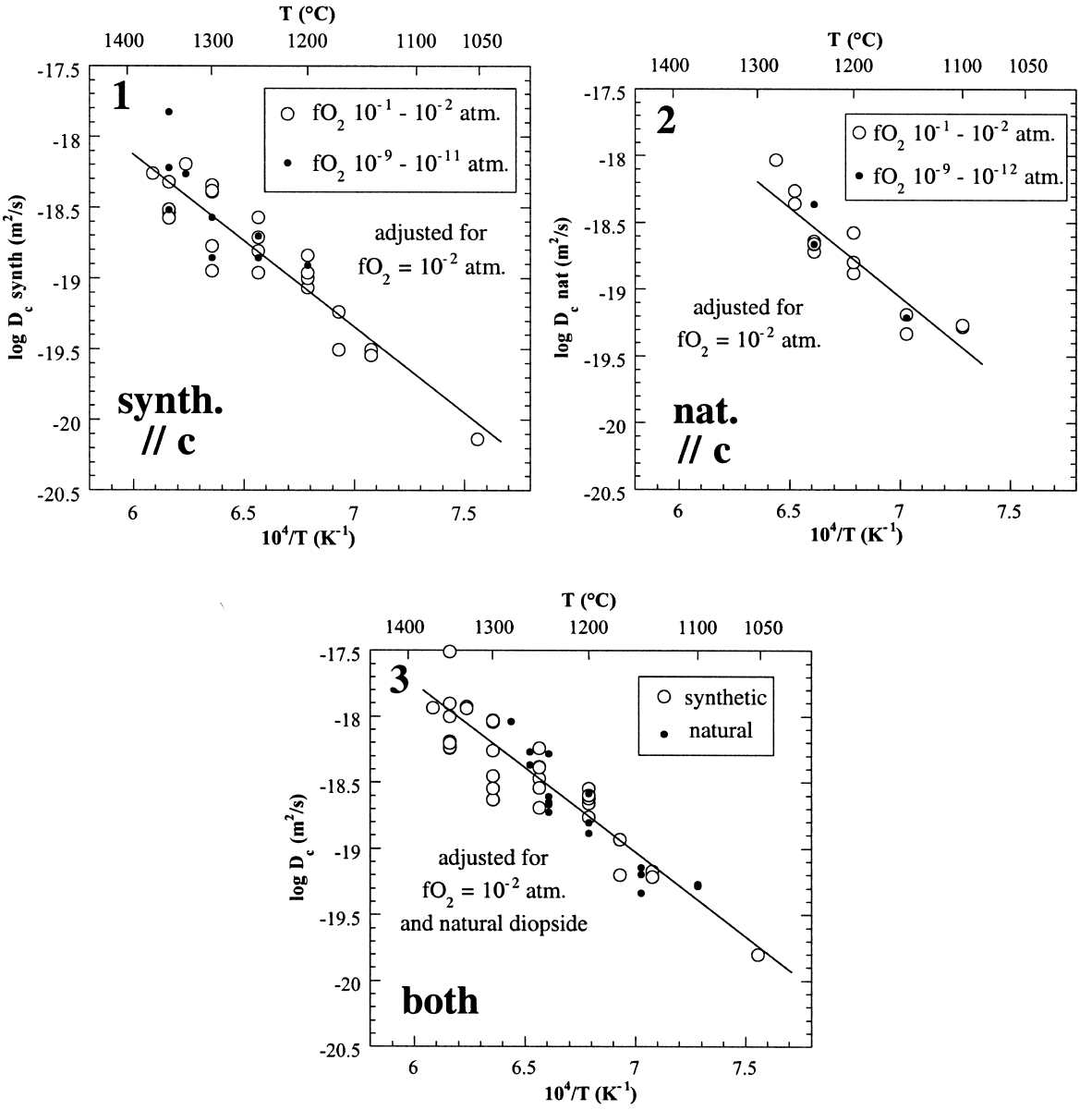

Fig. 6. Arrhenius plot of diffusion coefficients along c in synthetic (6.1) and natural (6.2) samples after correction of the fO_2 effect using Eqs. 7 and 8. (6.3) Gathers all synthetic and natural data with a correction of the shift between synthetic and natural sample using Eq. 9. Data are computed for $fO_2 = 10^{-2}$ atm.

samples (around a factor 2.2; Fig. 5). These data are best fitted by the equation:

$$\log D_c \text{ nat } (\text{m}^2\ \text{s}^{-1}) = -9.7 \pm 1.2 - (255 \pm 33\ \text{kJ mol}^{-1})/2.303\ RT \quad (6)$$

The results of oxygen diffusion in oxidizing conditions can be summarized as follows: D_c nat $\approx 2D_c$ synth $\approx 2D_a$ synth $\approx 20D_b$ synth.

3.2. Dependence of fO_2

A fO_2 change by eight to nine orders of magnitude has a very small effect on the diffusion coefficients along c in both synthetic and natural diopside. fO_2 does not seem to affect the activation energy of diffusion (Figs. 4.2 and 5). The effect is best fitted by the equations corresponding to Fig. 6.1, 6.2:

$$\log D_c \text{ synth } (\mathrm{m^2\ s^{-1}}) = -10.7 \pm 0.7 + 0.044 \log fO_2 - (234 \pm 19 \text{ kJ mol}^{-1})/2.303\ RT \quad (7)$$

$$\log D_c \text{ nat } (\mathrm{m^2\ s^{-1}}) = -9.5 \pm 1.1 + 0.031 \log fO_2 - (260 \pm 29 \text{ kJ mol}^{-1})/2.303\ RT \quad (8)$$

Thus, as shown in Figs. 4.2 and 5, the effect of fO_2 on diffusion along c does exist but is very small compared to the effect of temperature. The effect of fO_2 on diffusion along a direction might be apparently larger than along c (Fig. 4.2, 4.3 but we cannot conclude from only three data points at low fO_2 (Fig. 4.3).

3.3. Natural versus synthetic

Eqs. 7 and 8 have comparable activation energies and sensitivities to fO_2 suggesting a common mechanism of diffusion for synthetic and natural diopside. Thus it is possible to fit all the data along c by a single law which takes into account the shift $\delta\log D^{\text{synth/nat}}$ observed between synthetic and natural sample (Fig. 6.3):

$$\log D_c\ (\mathrm{m^2\ s^{-1}}) = -10.4 \pm 0.6 + 0.04 \log fO_2 - (246 \pm 15 \text{ kJ mol}^{-1})/2.303\ RT + \delta\log D^{\text{nat/synth}} \quad (9)$$

with $\delta\log D^{\text{nat/synth}} \approx +0.4$ in log unit in excess for natural compared to synthetic diopside.

This relationship allows transformation of the synthetic data into equivalent natural data in the temperature range of the study. It allows to fit the 51 data points altogether.

4. Discussion

4.1. Comparison with previous data: roles of anisotropy and water

The diffusion data collected by Ryerson and McKeegan (RMK) [8] from experiments performed at 1 atm under CO/CO_2 conditions, along c, are slightly but significantly lower than for our data from the natural diopside and their activation energy is higher too (Fig. 7). The differences cannot be explained by an effect of fO_2: this one is too small. An effect of composition is possible, but frequently diffusion in natural samples gives higher diffusion coefficients than in synthetic samples [17,22]. Moreover, RMK's data were col-

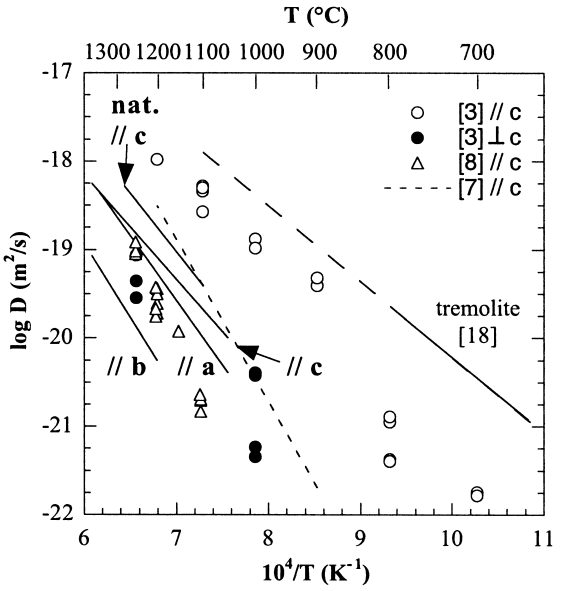

Fig. 7. Comparison with published data on oxygen diffusion in diopside. Full thin lines: present data, Eqs. 3–6), respectively for synthetic diopside //b, //a, //c and natural diopside //c. Upper full line: oxygen diffusion in tremolite // to c [18] with its extrapolation (thin dashed line).

lected from three diopsides from different origins and compositions and these authors observed no dependency with composition. However, we observe that RMK's data and ours converge when extrapolated toward 1400°C, this is in good agreement with the recently established compensation rule for oxygen diffusion in diopside [5].

4.1.1. Anisotropy

Our data confirm that diffusion of oxygen in diopside is anisotropic as already shown by Farver [3] who reports that *c* is a rapid direction and that diffusion is slow in a direction perpendicular to *c*, but which is not identified. We clearly show that there are two fast diffusion directions, *a* and *c*, and that *b* is slow. Farver's results [3] along the unknown direction perpendicular to *c* are 4× our value for *b* and 0.5× our value for *a*, suggesting that his diffusion direction was intermediate between *a* and *b*.

4.1.2. Water

Farver's results [3] for direction *c* are 10 times faster than ours: the difference is significant. His single crystals are almost pure diopsides and composition effect cannot be advocated to explain the observed discrepancy. The fO_2 conditions prevailing in his hydrothermal runs could also differ from ours but this cannot explain the factor of 10. Several authors [3,4,7] have interpreted the fast diffusion data of Farver along *c* as an effect of water fugacity fH_2O, ($fH_2O \approx 85$ MPa [18], while it is only around 0.0026 MPa in ours). However Farver's data and ours are similar for diffusion along directions perpendicular to *c* so that the argument of a direct influence of water fugacity upon diffusion seems dependent on crystallographic direction. In addition, hydrothermal runs performed by Elphick and Graham [6], with similar fH_2O (≈ 100 MPa) as Farver, reproduce values of *D* closer to ours for diffusion along *c* (dashed curve, Fig. 7).

One possible interpretation of the difference between Farver's experiments [3] and ours could be explained as follows. It is possible that the samples used by Farver could contain amphibole lamellae along (010) as it was recently observed by TEM on specimens from the same origin [19]. Spacing between lamellae may reach a few tens to hundred nanometer [19]. Lamellae could act as short circuits for diffusion in diopside along *c*. Faster diffusion along such amphibole lamellae could thus explain the fast diffusion observed along *c* in Farver's diopside specimens. In addition, it is also remarkable to notice that the set of data between 1200°C and 900°C reported in [3] for the *c* direction falls within the extrapolation of oxygen diffusion in tremolite amphibole [18], with an identical activation energy (slope, Fig. 7). If the above proposed explanation holds, the samples perpendicular to *c* in Farver's experiments should be more or less along *b*, i.e. perpendicular to the amphibole lamellae, a direction with diffusion only weakly affected by the presence of lamellae.

We conclude that the idea of a strong effect of water on diffusion of oxygen in diopside is not yet clearly demonstrated by experiments.

4.2. Anisotropy and crystallographic paths

As seen above, self-diffusion of oxygen in diopside is anisotropic with a rate of oxygen mobility 10 times smaller along *b*. The same anisotropic behavior has been previously observed in diopside for the diffusion of hydrogen present as point defect [20,21]. However, diffusion of cations like Ca [12,17], Sr [22], Fe [23] is isotropic. Yet, the diffusion of hydrogen is considerably faster than oxygen diffusion (at least by a factor of 10^{10}) and the activation energy of diffusion is half that of oxygen [20,21]. The particular behavior of hydrogen compared to other cations might be explained by the strong local bonding of interstitial hydrogen with oxygen, a situation that is different for cations that have their own site with high co-ordination number in oxygen polyhedra. In diopside there are three different oxygen sites: the bridging O3 oxygen has the largest binding energy (03 is chain forming) compared to the two non-bridging oxygens O1 and O2 [24,25] (Fig. 8). We suggest that the anisotropy observed for oxygen and hydrogen diffusion is related to the nature of the oxygen sites involved during the oxygen or hydrogen migration.

We show in Fig. 8 the three most probable

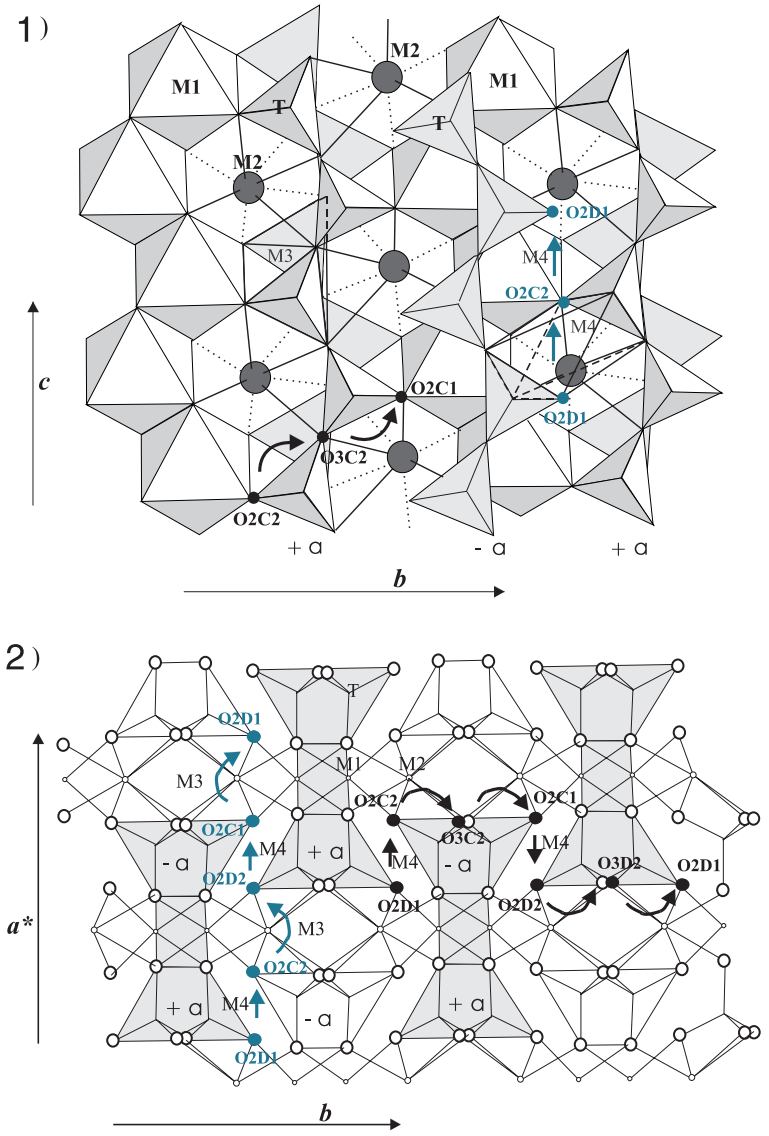

Fig. 8. Polyhedral drawing of the diopside structure showing the possible diffusion paths of oxygen along *c* (gray arrows in 8.1) and *a* (gray arrows in 8.2) directions using only O2 sites and along the *b* direction (black arrows in 8.1 and 8.2) using O2 and necessarily O3 bridging sites. (8.1) Structure projected along the *a** direction. (8.2) Structure projected along the *c* direction. M3 and M4 are empty polyhedral sites.

paths for oxygen migration in the three directions *c*, *a* and *b* assuming jumps from oxygen sites to sites. Paths along *c* and *a* directions only involve O2 sites but diffusion along *b* requires O3 sites in order to cross the tetrahedral chains (Fig. 8). Note that oxygen mobility in the structure may be facilitated by the presence of two empty octahedral interstitial sites, M3 and M4, already invoked earlier to interpret Ca diffusion [26].

4.3. Point defects

Compared with Ca diffusion in the same samples and within a same range of temperature

(1050–1370°C), oxygen shows only one regime of diffusion: there is no kink in the Arrhenius plot. The activation energies for oxygen diffusion (228–333 kJ mol^{-1}) are of the same order as for calcium in extrinsic regime (280 kJ mol^{-1} [11,17]). The energies of intrinsic defect formation such as oxygen Frenkel defects, or CaO or MgO Shottky defects [25] for instance are much too high relative to oxygen diffusion activation energy. Like most diffusion processes in minerals [27], oxygen diffusion in diopside is probably extrinsic. The existence of a dependence of D upon fO_2 proves it, even if we cannot decipher the cause.

4.4. Diffusion law for extrapolation to natural conditions

An important result of this study is the oxygen diffusion anisotropy: it has an important effect on how to interpret $^{18}O/^{16}O$ profiles found in diopside grains of cooled and uplifted rocks. Previous interpretations were done assuming only one fast direction of diffusion [3,4,8,10]. Such assumption is no longer valid and a 2D geometry of diffusion must be considered for the calculation of closure temperatures or cooling rates of rocks deduced from $^{18}O/^{16}O$ profiles in clinopyroxenes. Cooling rates may be underestimated by a large factor (at least 2) if the proper anisotropy of diffusion is not used in calculations [11].

The strong anisotropy, with two rapid directions, means that these two directions a and c will dominate the $^{18}O/^{16}O$ exchange between small diopside grains embedded in a large rock-reservoir. As diffusion along a and c have very similar laws (Eqs. 4 and 5 for synthetic), we propose to use the following double law for natural samples:

$$\log D_{a,c} = -10.0 \pm 0.6 + 0.04 \log fO_2 - (246 \pm 15 \text{ kJ mol}^{-1})/2.303\ RT \quad (10)$$

together with $D_b \ll D_{a,c}$, so that in a 3D diffusion $\log D_{a,c}$ dominates.

The conditions of oxygen fugacity within much of the high-grade metamorphic terrains where clinopyroxene may be used as geospeedometer are roughly defined by the QFM equilibrium within ± 3 log units [28]. The effect of the error on the exact location relative to the QFM equilibrium does not play significant role either. However, a change of fO_2 with temperature along QFM is more important (fO_2 changes by 11 log units between 500 and 900°C, [29]). To extrapolate the diffusion law to natural conditions buffered at QFM we must include into Eq. 10 the equation of the buffer [29]:

$$\log fO_2 = -24441.9/T + 8.290 \quad (11)$$

It yields an apparent activation energy $E^* = 259$ kJ mol^{-1} at QFM conditions:

$$\log D_{a,c} = -10.0 \pm 0.6 - (259 \pm 15 \text{ kJ mol}^{-1})/2.303\ RT \quad (12)$$

Eq. 11 is strictly valid for temperatures above 575°C, and another fO_2 versus T law should be used between 575°C and 25°C [29]. However, the difference between these two laws is practically negligible down to 300°C. Eq. 12 was obtained by assuming E^* independent of T (E^* was computed for $T = 650$°C). We also assumed no effect of pressure on the QFM equilibrium, for such effect is expected to be less than 1 log unit of fO_2 over a range of 1 GPa [30]. The effect of all these approximations is far below the uncertainty on D_0 (± 0.6) or E^* (± 15 kJ mol^{-1}). The simple diffusion law (Eq. 12) can be easily used for any computation of $^{18}O/^{16}O$ profiles in natural diopsides. It is represented in Fig. 9 and is compared with all experimental data.

It is interesting to note that the diffusion coefficients predicted from Eq. 12 for the two fast directions are in good agreement with the empirical estimation of the upper limit of diffusion coefficients deduced from the absence of isotopic variation in natural diopside grains studied in marbles of the Cascade Slide area (Adirondack Mountains) [10] (rectangular area in Fig. 9). The limit was deduced from the lack of evidence of oxygen diffusion in diopside grains with a diameter size as small as 0.3 mm. The peak temperature of the metamorphic event and the rate of the sub-

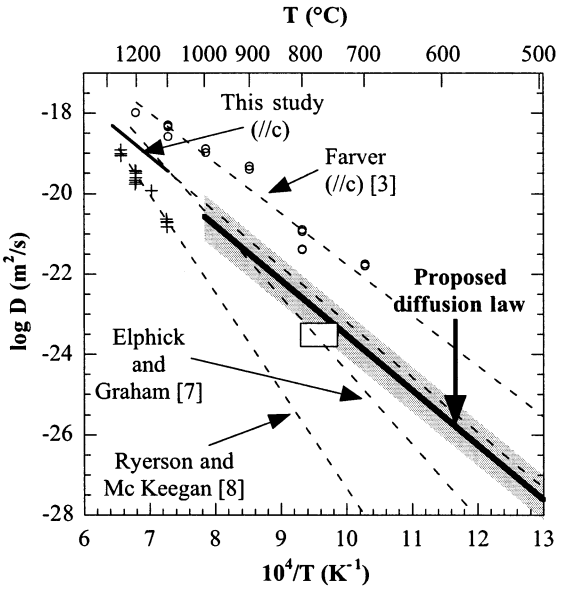

Fig. 9. Arrhenius plot of Eq. 12 proposed for the extrapolation to natural samples with its uncertainty (shadow), compared to most of experimental data and their direct extrapolations toward low temperature ([3,7,8] and this study). The small rectangular domain corresponds to an estimate made by Sharp and Jenkins [10] corresponding to the lower limit of D that could be observed in natural diopside grains with size = 0.3 mm. This value agrees with the proposed log D versus $1/T$ relation represented by the solid line.

sequent cooling were estimated to 770 ± 30°C and 1–2°C/Ma [31]. The authors [10] estimated the upper limit of the diffusion coefficient to be 1–5.6×10^{-24} m^2 s^{-1} from the computation of the closure temperature using Dodson's equation [32].

5. Conclusion

The oxygen diffusion experiments performed between 1050 and 1370°C in the three principal crystallographic directions in a synthetic diopside, demonstrate the evidence of only one slow direction, b, and two fast, a and c. The slowest diffusion along b is due to the difficulty of oxygen atoms to cross the SiO_4 chains of the diopside structure through the strongly bonded O3 oxygen sites. Diffusion along b is insensitive to oxygen fugacity, while it is weakly dependent on fO_2 for a and c. The low activation energies found (between 228 and 323 kJ mol^{-1}) are compatible with an extrinsic regime of diffusion. We suggest that $^{18}O/^{16}O$ kinetic equilibration in diopside grains is controlled at QFM buffer conditions by the simple laws:

$$\log D_{a,c} = -10.0 \pm 0.6 - (259 \pm 15 \text{ kJ mol}^{-1})/$$

$$2.303\,RT \text{ and } D_b \ll D_{a,c}.$$

Acknowledgements

This work was supported by the CNRS-INSU (INSU contribution number 427, program 97 IT 62; GDR 86 directed by G. Amsel). We would like to thank R. Freer, J. Craven and F. Azough for SIMS measurements on one of our samples. F. Abel and I. Vickridge are greatly acknowledged for their help during the NRA analyses. S. Elphick is acknowledged for a very constructive review. *[BW]*

References

[1] B.J. Giletti, Diffusion effects on oxygen isotope temperatures of slowly cooled igneous and metamorphic rocks, Earth Planet. Sci. Lett. 77 (1986) 218–228.
[2] J.M. Eiler, L.P. Baumgartner, J.W. Valley, Fast grain boundary a fortran-77 program for calculating the effect of retrograde interdiffusion of stable isotopes, Comput. Geosci. 20 (1994) 1415–1434.
[3] J.R. Farver, Oxygen self-diffusion in diopside with application to cooling rate determinations, Earth Planet. Sci. Lett. 92 (1989) 386–396.
[4] K.J. Edwards, J.W. Valley, Oxygen isotope diffusion and zoning in diopside: The importance of water fugacity during cooling, Geochim. Cosmochim. Acta 62 (1998) 2265–2277.
[5] O. Jaoul, F. Béjina, Diffusion and Geophysics: geospeedometry and compensation rule, in: Defects and diffusion forum, Trans. Tech. Publ., Ueticon–Zürich, 2001, pp. 983–999.
[6] O. Jaoul, V. Sautter, A new approach to geospeedometry based on the 'compensation law', Phys. Earth Planet. Inter. 110 (1999) 95–114.
[7] S.C. Elphick, C.M. Graham, Hydrothermal oxygen diffusion in diopside at 1kb, 900–1200°C, a comparison with oxygen diffusion in forsterite, and constraints on oxygen

isotope equilibrium in peridotite nodules, Terra Abstr. 2 (1990) 8.
[8] F.J. Ryerson, K.D. McKeegan, Determination of oxygen self-diffusion in akermanite, anorthite, diopside, and spinel: Implication for oxygen isotopic anomalies and the thermal histories of Ca–Al-rich inclusions, Geochim. Cosmochim. Acta 58 (1994) 3713–3734.
[9] L. Pacaud, J. Ingrin, O. Jaoul, High-temperature diffusion of oxygen in synthetic diopside measured by nuclear reaction analysis, Mineral. Mag. 63 (1999) 673–686.
[10] Z.D. Sharp, G.R.T. Jenkin, An empirical estimate of the diffusion rate of oxygen in diopside, J. Metamorph. Geol. 12 (1994) 89–97.
[11] L. Pacaud, Mesure de l'autodiffusion de l'oxygène et du magnésium dans le diopside et applications, Ph.D. Thesis Université de Paris-Sud Orsay, France, 1999.
[12] A. Dimanov, J. Ingrin, Premelting and high-temperature diffusion of Ca in synthetic diopside: An increase of the cation mobility, Phys. Chem. Minerals 22 (1995) 437–442.
[13] J. Ingrin, S. Hercule, T. Charton, Diffusion of hydrogen in diopside: Results of dehydration experiments, J. Geophys. Res. 100 (1995) 15489–15499.
[14] O. Jaoul, B. Houlier, F. Abel, Study of ^{18}O diffusion in magnesium orthosilicate by nuclear microanalysis, J. Geophys. Res. 88 (1983) 613–624.
[15] A.C.S. Sabioni, F.L. Freire Jr, C.V. Barros-Leite, B.A. Amami, C. Dolin, C. Monty, F. Millot, Study of oxygen self-diffusion in oxides by ion beam techniques: comparison between nuclear reaction and SIMS, Nuclear-Instr. Methods Phys. Res. B73 (1993) 85–89.
[16] O. Gérard, O. Jaoul, Oxygen Diffusion in San Carlos Olivine, J. Geophys. Res. 94 (1989) 4119–4128.
[17] A. Dimanov, O. Jaoul, V. Sautter, Calcium self-diffusion in natural diopside single crystals, Geochim. Cosmochim. Acta 60 (1996) 4095–4106.
[18] J.R. Farver, B.J. Giletti, Oxygen diffusion in amphiboles, Geochim. Cosmochim. Acta 49 (1985) 1403–1411.
[19] J. Ingrin, K. Latrous, J.C. Doukhan, N. Doukhan, Water in diopside: an electron microscopy and infrared spectroscopy study, Eur. J. Mineral. 1 (1989) 327–341.
[20] S. Hercule, J. Ingrin, Hydrogen in diopside: Diffusion, kinetics of extraction–incorporation, and solubility, Am. Mineral. 84 (1999) 1577–1587.
[21] S.C. Woods, S. Mackwell, D. Dyar, Hydrogen in diopside: Diffusion profiles, Am. Mineral. 85 (2000) 480–487.
[22] M. Sneeringer, S.R. Hart, N. Shimizu, Strontium and samarium diffusion in diopside, Geochim. Cosmochim. Acta 48 (1984) 1589–1608.
[23] F. Azough, R. Freer, Iron diffusion in single-crystal diopside, Phys. Chem. Minerals 27 (2000) 732–740.
[24] S. Sasaki, K. Fujino, Y. Takeuchi, R. Sadanaga, On the estimation of atomic charge by X-ray method for some oxides and silicates, Acta Crystallogr. 36 (1980) 904–915.
[25] F. Azough, R. Freer, K. Wright, R. Jackson, A computer simulation study of point defects in diopside and the self-diffusion of Mg and Ca by a vacancy mechanism, Miner-al. Mag. 62 (1998) 599–606.
[26] A. Dimanov, O. Jaoul, Calcium self-diffusion in diopside at high temperature: implications for transport properties, Phys. Chem. Minerals 26 (1998) 116–127.
[27] R. Freer, Diffusion in silicate minerals and glasses: A data digest and guide to the literature, Contrib. Mineral. Petrol. 76 (1981) 440–454.
[28] D.R. Lentz, Late-tectonic U–Th–Mo–REE skarn and carbonitic vein–dyke systems in the southwestern Grenville province: A pegmatite-related pneumatolytic model linked to marble melting (limestone syntexis), Mineral. Assoc. Canada Short Course Handb. 26 (1998) 519–657.
[29] J. Myers, H.P. Eugster, The system Fe–Si–O: Oxygen buffer calibrations to 1500 K, Contrib. Mineral. Petrol. 82 (1983) 75–90.
[30] D.A. Hewitt, A redetermination of the fayalite–magnetite–quartz equilibrium between 650 and 850°C, Am. J. Sci. 278 (1978) 715–724.
[31] K. Mezger, C.M. Rawnsley, S.R. Bohlen, G.N. Hanson, U–Pb garnet, sphene, monazite and rutile ages: implications for the duration of high-grade metamorphim and cooling histories, Adirondack Mts., New York, J. Geol. 99 (1991) 415–428.
[32] M.H. Dodson, Closure temperature in cooling geochronological and petrological systems, Contrib. Mineral. Petrol. 40 (1973) 259–274.